Ultrafast Science
A SCIENCE PARTNER JOURNAL

RESEARCH ARTICLE

Highly Sensitive and Fast Hydrogen Detection Based on Light-Induced Thermoelastic Spectroscopy

Yufei Ma*, Tiantian Liang, Shunda Qiao, Xiaonan Liu, and Ziting Lang

National Key Laboratory of Science and Technology on Tunable Laser, Harbin Institute of Technology, Harbin 150001, China.

*Address correspondence to: mayufei@hit.edu.cn

Citation: Ma Y, Liang T, Qiao S, Liu X, Lang Z. Highly Sensitive and Fast Hydrogen Detection Based on Light-Induced Thermoelastic Spectroscopy. *Ultrafast Sci.* 2023;3:Article 0024. https://doi.org/10.34133/ultrafastscience.0024

Submitted 30 December 2022
Accepted 13 March 2023
Published 29 March 2023

As a new energy source, hydrogen (H_2) detection is a hot topic in recent years. Because of the weak absorption characteristic, laser spectroscopy-based H_2 detection is challenging. In this paper, a highly sensitive H_2 sensor based on light-induced thermoelastic spectroscopy (LITES) technique is demonstrated for the first time. A continuous-wave, distributed feedback diode laser with emission in the 2.1 μm region was adopted as the excitation source to target the strongest H_2 absorption line of 4,712.90 cm^{-1}. A Herriott multipass cell with an optical length of 10.1 m was chosen to further improve the H_2 absorption. With the feature of processing the raw input data without data preprocessing and extracting the desired features automatically, the robust shallow neural network (SNN) fitting algorithm was brought in to denoise the sensor. For the LITES-based H_2 sensor, the concentration response was tested, and an excellent linear response to H_2 concentration levels was achieved. A minimum detection limit (MDL) of ~80 ppm was obtained. On the basis of implementation of the H_2-LITES sensor, a heterodyne H_2-LITES sensor was further constructed to realize a fast measurement of resonance frequency of quartz tuning fork and H_2 concentration simultaneously. The resonance frequency can be retrieved in several hundred milliseconds with the measurement accuracy of ±0.2 Hz, and the result of 30,713.76 Hz is exactly same as the experimentally determined value of 30,713.69 Hz. After the SNN algorithm was applied, an MDL of ~45 ppm was achieved for this heterodyne H_2-LITES sensor.

Introduction

With the rapid development of the industry, the rate of energy consumption becomes fast. However, the traditional fossil fuels such as coal and oil produce a large number of pollutants in the combustion process [1]. Hydrogen (H_2) has the merits of clean and renewable, as representative of new energy [2]. The product of H_2 combustion is water vapor (H_2O), which is environmentally friendly. Therefore, H_2 enables switch from a fossil fuel-based industry to a clean energy-based industry [3]. However, H_2 is dangerous. It is an explosive and flammable gas. When the volume fraction of H_2 exceeds 4% in air, it has a risk of explosion. With its colorless and odorless characteristics, human cannot sense H_2. Hence, there is a great need of sensitive and selective detection of H_2 in the processes of production, transportation, storage, and usage [4].

Various sensors have been reported for H_2 detection. The electrochemical kind relies on the change of electrical characteristics such as resistance and current [5]. It has a miniature size and low cost. However, the poor long-term stability and detection performance limit its application. A catalytic combustion method-based gas sensor reacts with the flammable H_2 [6,7]. However, it requires a high operation temperature (>100 °C) and therefore has some risks. In the functional material-based H_2 sensing, palladium (Pd) film is widely adopted. However, this kind of sensor has the weakness of poor repeatability, complicated synthesis, and unexpected drift [8,9]. Moreover, the vibration of a quartz resonator [10]- or a cantilever beam [11]-based mechanical sensor, the surface acoustic wave [12]- or sound velocity [13]-based acoustic sensor, and the surface plasmon resonance [14]- or the shift of transmission/reflection wavelength [15]-based optical sensor is also adopted on some occasions. Unfortunately, the mechanical sensors have some difficulties in fabrication. The acoustic sensors are susceptibly interfered by the environmental sound. The optical sensors are easily disturbed by stray light and vibrations.

Unlike the abovementioned techniques, the laser spectroscopy-based gas sensing method is based on the molecular fingerprint spectrum of light absorption [16,17]. It has the advantages of high selectivity, high sensitivity, and on-line measurement ability [18–20]. Laser spectroscopy-based gas sensors can be classified into 3 types: (a) tunable diode laser absorption spectroscopy (TDLAS)-based measurement; (b) cavity-enhanced absorption spectroscopy-based measurement; and (c) photothermal, photoacoustic, and other laser spectroscopy-based measurement. On the basis of the Beer–Lambert law, in TDLAS and cavity-enhanced absorption spectroscopy, a photodetector is used to measure the optical signal [21,22]. In the years 2019 and 2022, a TDLAS-based H_2 measurement was performed [23,24]. However, the photodetector is usually bulky and expensive, especially for those used in the mid-infrared region, such as a mercury cadmium telluride photodetector with cryogenic cooling unit. Furthermore, in the >10-μm spectral region, the optical detectors are basically unavailable. In the year 2002, as a modification to the traditional microphone-based photoacoustic spectroscopy, quartz-enhanced photoacoustic spectroscopy (QEPAS) was put forward [25]. A quartz tuning fork (QTF) with piezoelectric property is adopted to detect acoustic waves in QEPAS. The characteristics of a high Q factor (>10,000), narrow frequency bandwidth (~3 Hz), low cost (<$1), tiny volume (~3 mm^3), and acoustic quadrupole geometry of QTF improve the detection performance, compactness, and cost of QEPAS-based sensors [26–29], and this technique has been used in numerous trace gas detections [30–35]. However, the QTF needs to be immersed in the gas environment, which means that QEPAS is a contact measurement method. When encountering acidic or corrosive gases, such as hydrogen chloride [36], the silver layer on the surface of QTF acting as an electrode can be easily corroded after a long time exposure, which will finally lead to sensor failure.

To solve the problem existing in QEPAS, light-induced thermoelastic spectroscopy (LITES) was first proposed in 2018 [37]. In LITES, the laser beam is focused on the surface of QTF after passing through the gas sample. Thermal expansion occurs in QTF because part of the laser energy is absorbed by it [38,39]. Mechanical motion is generated along with thermal expansion, and this motion is amplified by the intrinsic resonance characteristic of QTF [40]. Finally, because of the piezoelectric property of QTF, the mechanical motion converts into an electrical signal, which is used to retrieve the gas concentration. In LITES, QTF does not need to put in the gas sample. Therefore, it is a noncontact measurement technique [41]. Furthermore, compared with the photodetector employed in the TDLAS method, QTF has no response wavelength limit. Because of these merits, LITES are extensively used in trace gas detection [42–45].

The resonance frequency (f_0) of QTF determines the laser modulation frequency and harmonic signal demodulation frequency, and it only has a narrow bandwidth of ~3 Hz [46]. Therefore, it is a key parameter for LITES-based gas sensing, and usually, it should be calibrated frequently, especially when environmental factors such as temperature and pressure change. There are 2 methods of optical and electrical excitations to measure the resonance frequency. In these 2 approaches, the excitation frequency of light and sinusoidal wave scans in a wide range, which means that the measuring is several minutes and time consuming, respectively. Furthermore, during this measuring process, the sensor should be suspended. Heterodyne detection of QEPAS sensor was first reported in 2017 [47]. In this method, the information of QTF such as f_0 can be obtained with the gas concentration simultaneously without interrupting sensing.

In this paper, a highly sensitive H_2 sensor based on LITES technique is demonstrated for the first time. To fix the issue of very weak absorption, a continuous-wave, distributed feedback (CW-DFB) diode laser with an emitting wavelength of 2.1 μm was adopted to target the strongest absorption line of H_2. Furthermore, a Herriott multipass cell (MPC) with an optical length of 10.1 m was employed to improve the optical absorption. A heterodyne H_2-LITES sensor was further constructed to realize a fast measurement of resonance frequency of QTF and H_2 concentration simultaneously.

Experimental system

H_2 absorption line selection

Because of its symmetric molecule structure, H_2 has a small number of absorption lines. Because these lines have a very weak absorption line strength (in the order of 10^{-26} cm^{-1}/cm^{-2} × molec), it is a big challenge for H_2 detection using laser spectroscopy-based methods. On the basis of the HITRAN 2020 database [48], the absorption lines of H_2 are simulated at the conditions of 760 torr of pressure and 300 K of temperature and are presented in Fig. 1A. In these few lines, it is found that the strongest one is located at 4,712.90 cm^{-1} with a line strength of 3.17 × 10^{-26} cm^{-1}/cm^{-2} × molec. To clarify the absorption interference from other molecules, 2% H_2O and 200 ppm of carbon dioxide (CO_2) were added around 4,712.90 cm^{-1}. It can be observed from Fig. 1B that, with an optical length (L) of 10 m, the absorbance of H_2 and H_2O are 1.86 × 10^{-4} and 5.80 × 10^{-4}, respectively, and the absorbance of CO_2 is negligible. Furthermore, it is can also be observed that H_2 is free from spectral interference of H_2O and CO_2. Therefore, in the following experimental investigations, the H_2 absorption line of 4,712.90 cm^{-1} is selected.

Diode laser output characteristics

For the sake of targeting the strongest absorption line of H_2 selected in the "H_2 absorption line selection" section, a CW-DFB diode laser (model no.: NP-DFB-2122-TO5-HC, Nanoplus GmbH) with an emission wavelength of 2.1 μm was adopted. This laser is in a TO5 package including a thermoelectric control (TEC). The output performance of this laser is tested and depicted in Fig. 2. At 3 different TEC temperatures of 35, 37, and 39 °C, the emission wavelength and output power were recorded. As presented in Fig. 2A, the experimentally determined current and temperature tuning coefficients of the laser wavelength were −0.061 cm^{-1}/mA and −0.46 cm^{-1}/°C, respectively. The TO5 package has a limited heat dissipation capability. To protect this laser from thermal damage and to prolong its service life, a TEC temperature of 39 °C is chosen in the following experiments to ensure that it does not have a

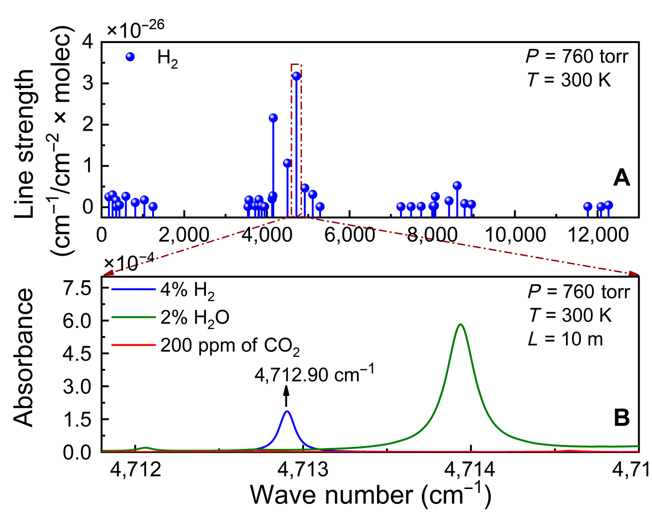

Fig. 1. Absorption spectra simulation according to the HITRAN 2020 database. (A) Line strength for all H_2 absorption lines. (B) Absorbance for 4% H_2, 2% H_2O, and 200 ppm of CO_2 at a pressure of 760 torr, a temperature of 300 K, and an optical length of 10 m.

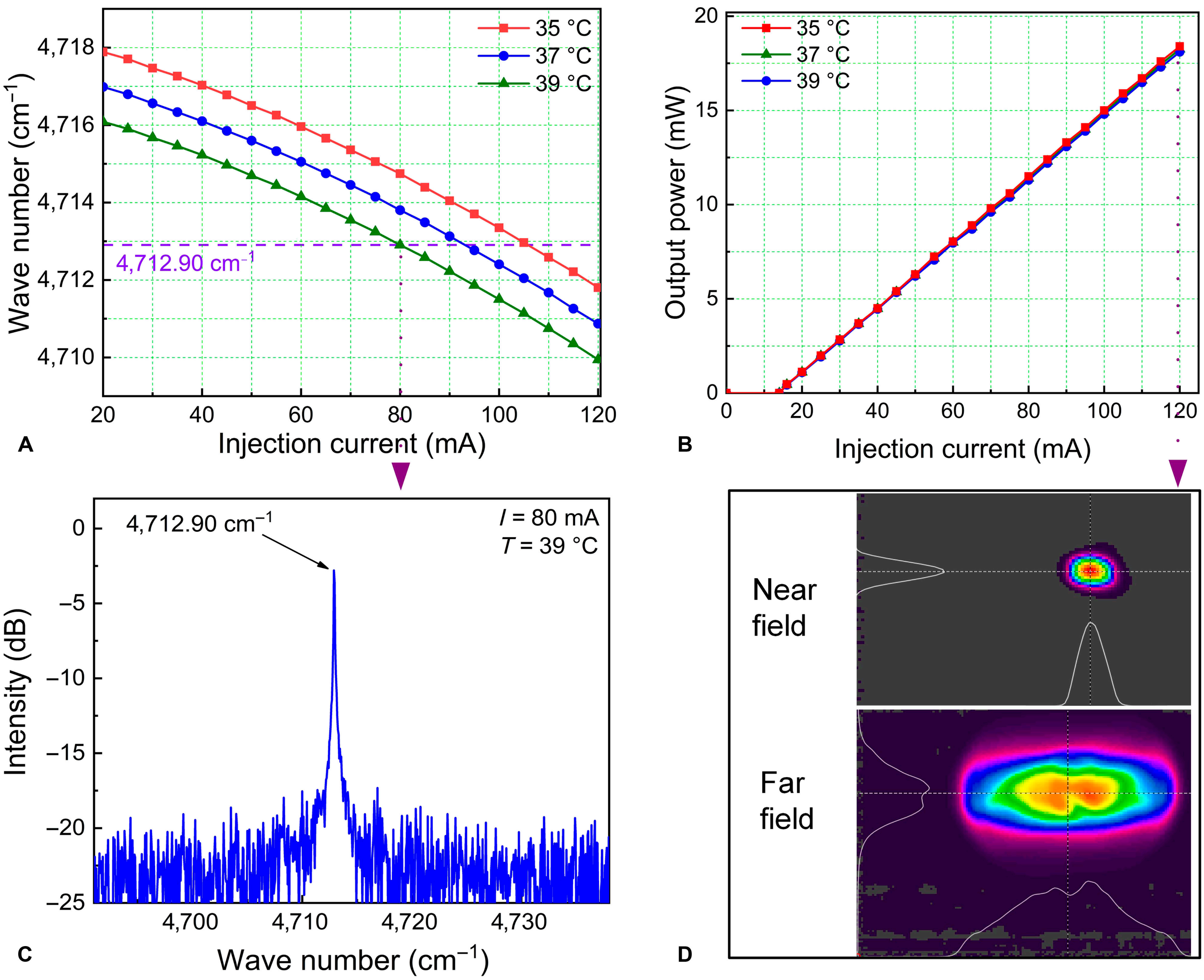

Fig. 2. Output performance of the 2.1 μm CW-DFB diode laser. (A) Current and temperature determined wavelength tuning. (B) Output power versus injection current. (C) Emission spectrum. (D) Distributions of the near and far fields of the beam profile.

high injection current. As depicted in Fig. 2B, the temperature has a weak influence on the output power, and the maximum optical power of 18.4 mW is obtained when the diode laser operates at an injection current of 120 mA. The emission wavelength of this diode laser is tuned to the H_2 absorption line of 4,712.90 cm^{-1}, as depicted in Fig. 2C, when the TEC temperature is 39 °C and the injection current is 80 mA. It is observed that the side–mode suppression ratio is higher than 20 dB. The output beam is collimated using an aspherical lens with a focal length of 5.95 mm and an antireflection coating. The distributions of the near and far fields of the beam profile were measured by employing a pyroelectric array camera at the 120 mA maximum injection current and are shown in Fig. 2D. Because of the different divergence speeds in the fast and slow axes of the diode laser adopted, the output laser beam profile shows symmetrically circular distribution in the near field while an asymmetrical elliptical distribution in the far field.

Sensor structure

A schematic diagram of the LITES-based H_2 sensor is depicted in Fig. 3. After passing through an aspherical lens (L1) with a focal length of 5.95 mm, the light beam of the 2.1 μm diode laser was collimated and incident into a Herriott MPC. With 34 optical passes and a 34 cm physical length, the MPC has an effective optical path length of 10.1 m. Using a calcium fluoride plano-convex lens (L2) with a focal length of 30 mm, the laser emitted from the MPC was focused onto the bottom of QTF, where the QTF could generate the maximum strain field [49]. A QTF with a resonance frequency (f_0) of 30.72 kHz (in vacuum) was used in the experiments as a light thermoelastic transducer. Compared to the widely used 32.768 kHz of QTF, this QTF has a lower f_0, which is in favor of increasing the energy accumulation in QTF and the sensor signal amplitude [50]. Two mass controllers (model no.: SC117 D07−19B, Beijing Sevenstar Co. Ltd.) with an uncertainty of ±3% were employed to mix pure H_2 with pure nitrogen (N_2) in different ratios to produce H_2 gas with different concentration levels, and the gas was fed into the MPC at a flow rate of 180 ml/min. Two reducing valves that were used to maintain the gases from gas cylinders were in normal pressure. Wavelength modulation spectroscopy (WMS) with the harmonic detection method was taken to realize a sensitive measurement of the H_2-LITES sensor signal. In

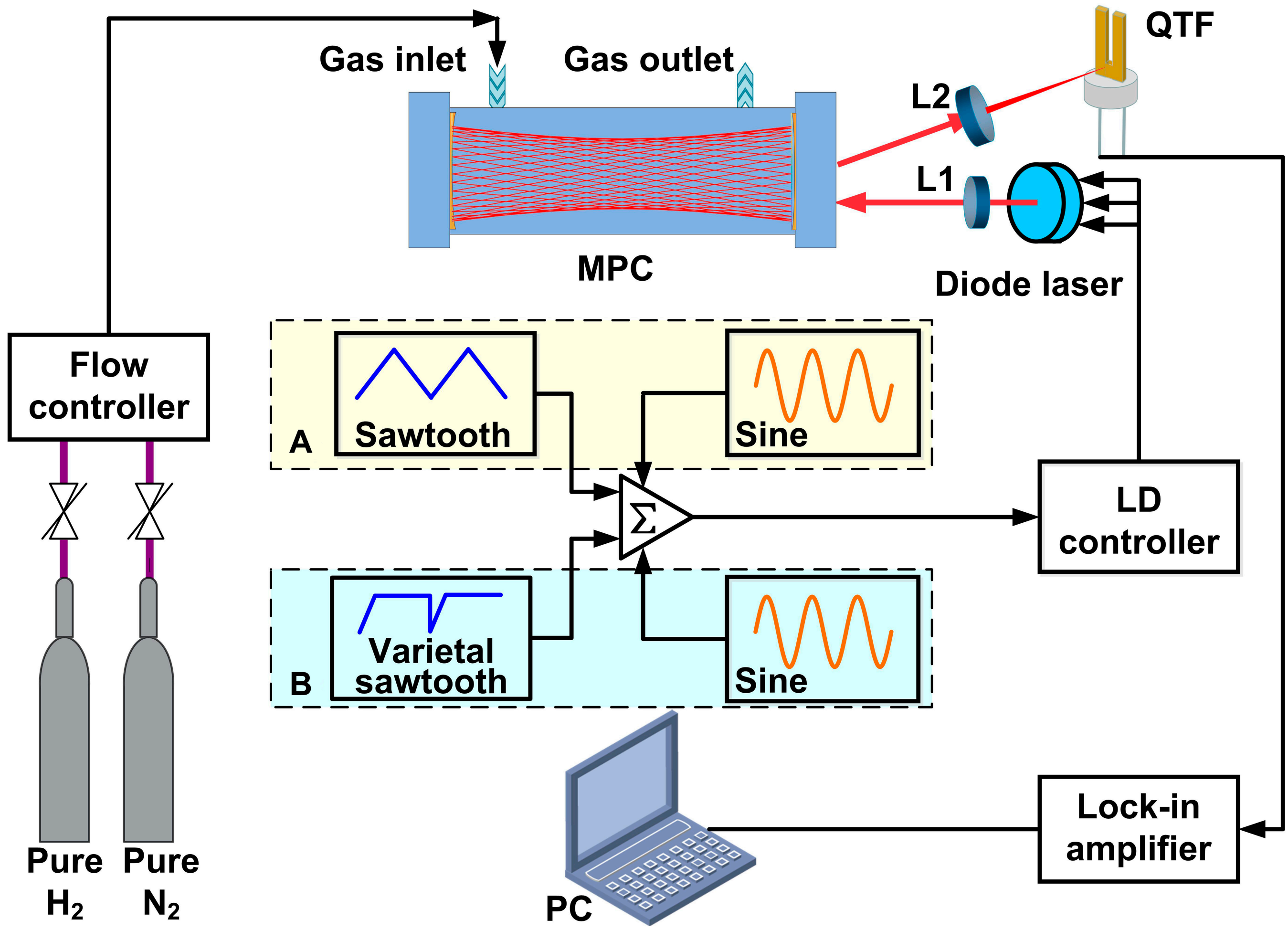

Fig. 3. Schematic of the LITES-based H_2 sensor platform. (A) Wavelength modulation mode for the LITES system. (B) Wavelength modulation mode for heterodyne LITES system. QTF, quartz tuning fork; Σ, adder; MPC, multipass cell; L1, lens; L2, lens; PC, personal computer; LD, laser diode.

WMS, a low-frequency sawtooth wave and a high-frequency sine wave are added together through the adder and then sent into the laser controller to modulate the laser wavelength. The sawtooth wave is used to scan across the selected H_2 absorption line. The sine wave is applied to modulate the laser absorption to produce the signal and reduce the background noise of the sensor system. In a normal LITES sensor system, as shown in the inset of Fig. 3A, because of the limitation of response frequency of QTF and the requirement of a long time to accumulate weak thermoelastic energy, usually, the period of the sawtooth wave is in several minutes. In the heterodyne LITES sensor system, the modulation frequency of laser is far from the resonance frequency of QTF. In such condition, a beat frequency signal is produced between the nonresonance frequency modulation and the transient response of QTF in the resonance state. This transient process needs a fast wavelength scanning. Therefore, as shown in the inset Fig. 3B, a varietal sawtooth wave with a fast sweep phase and a stable phase is used. The fast sweep phase has a time scale in several hundred milliseconds and is intended to offer an impulse to the QTF. The stable phase has a pretty long period and is used to acquire the ring-down process of the heterodyne LITES signal.

Results and Discussion

LITES-based H_2 sensing

The resonance frequency (f_0) of QTF determines the modulation frequency of the laser and, therefore, should be accurately measured. In this research, an optical excitation method was used to fix it. The laser excitation frequency was scanned from 30,708 to 30,728 Hz. Because of the requirements of the steady-state response of QTF and accurate measurement, the measuring process lasted 100 s and the f_0 was determined to be 30,718.38 Hz. As shown in Fig. 4, the detection bandwidth was found to be $\Delta f_0 = 3.6$ Hz. On the basis of the equation: $Q = f_0 / \Delta f_0$, the quality factor (Q) was calculated as 8,533. The measured equivalent resistance of the used QTF was 112.98 kΩ. In the following experiments, WMS with the second harmonic (2f) detection strategy was employed. Therefore, the laser modulation frequency f should be set as $f = f_0/2 = 15{,}359.19$ Hz.

The signal level of the LITES sensor is related to the laser wavelength modulation depth. Hence, the modulation current (sine wave amplitude) for the H_2-LITES sensor was investigated at the H_2 concentration of 100%, and the results are presented in Fig. 5. At the beginning, the 2f signal amplitude of the H_2-LITES sensor increased with the modulation current. After

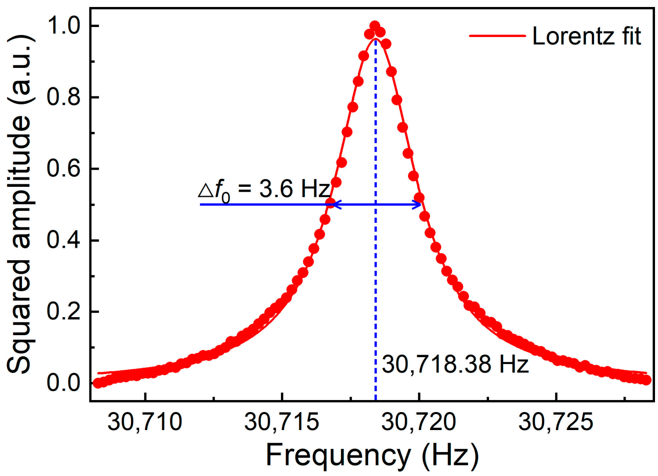

Fig. 4. The frequency response curve of the used QTF. a.u., arbitrary units.

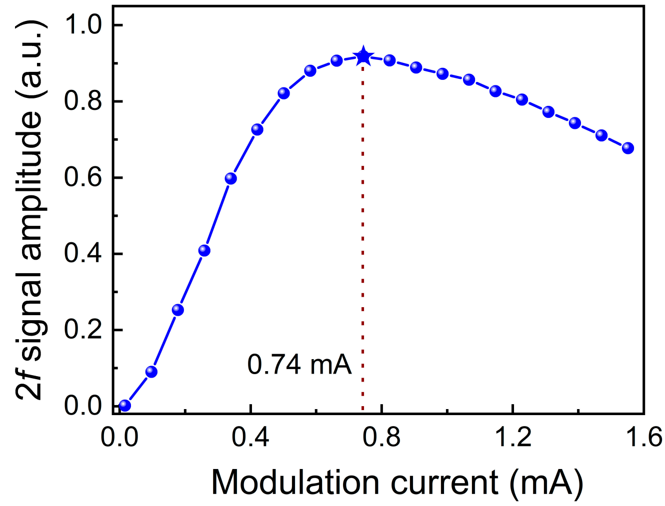

Fig. 5. The *2f* signal amplitude of H_2-LITES sensor versus laser modulation current.

that, the 2*f* signal amplitude began to decrease. The maximum 2*f* signal level is achieved when the modulation current is 0.74 mA. Therefore, in the following investigations, this optimum value is adopted.

The sensor performance was evaluated using H_2 with different concentrations when the integration time of the lock-in amplifier (model no.: MFLIDC-500 kHz, Zurich Instruments) was set to 700 ms. The pure H_2 was diluted with pure N_2 to generate different gas samples with concentration ranging from 100% to 10%. The obtained 2*f* signal waveforms are shown in Fig. 6A. To investigate the linear response of the LITES-based H_2 sensor, the obtained 2*f* signal amplitude versus H_2 concentration is depicted in Fig. 6B. After linear fitting, the R^2, which implies how well the regression line approaches real data points, is found to be 0.99. This reflects that the H_2-LITES sensor has an outstanding linear response to H_2 concentration levels.

The noise level of the H_2-LITES sensor is measured when the injection current (wavelength) is far from the absorption line. The right wing of the H_2-LITES 2*f* signal is used to calculate the noise. For the purpose of reducing the system noise level and to further improve the detection performance, the shallow neural network (SNN) is adopted, which has a simple structure and is proved to be an end-to-end method. This fitting algorithm processes the raw input data without any data preprocessing and can automatically extract the desired features [51,52]. The fitting based on SNN is achieved by automatically learning the features between input data X and output data Y in the dataset, adjusting the weight and bias of the neurons in the hidden layer and output layer based on the characteristics of these data, and then accumulating a series of neurons in the the form of an activation function. Five layers were included within the hidden layer. The training data, test data, and validation data account for 70%, 15%, and 15% of the data that were set, respectively. In the subsequent noise reduction processing, the minimum root mean square error is used as the criterion. When the mean square error between the original data and the

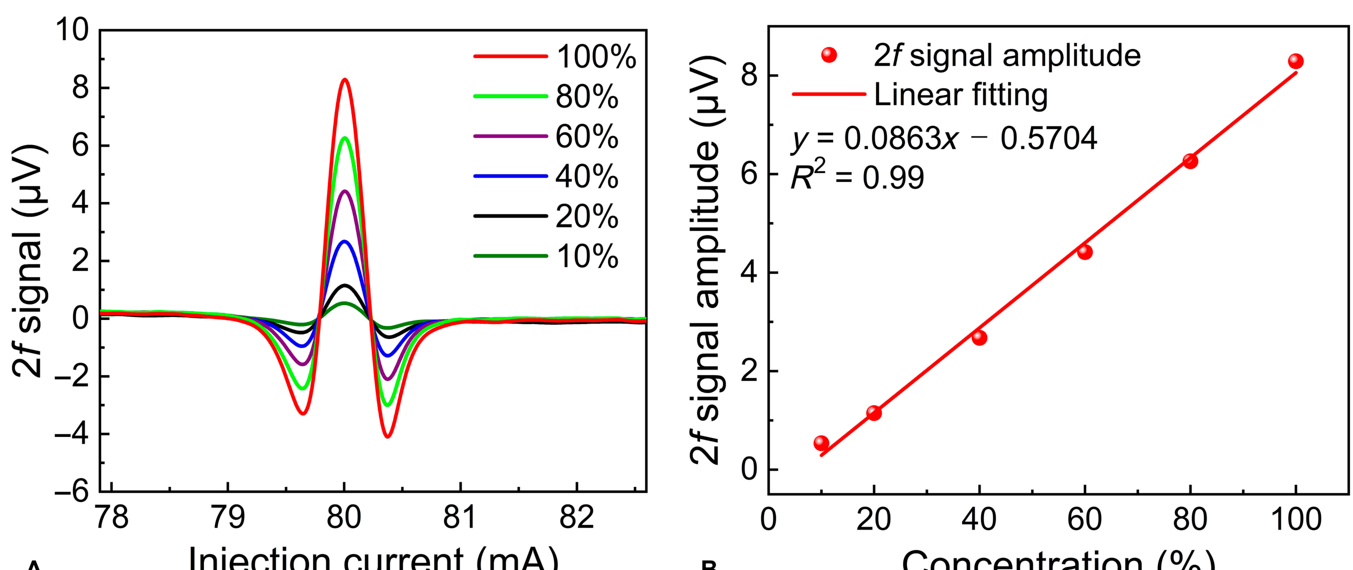

Fig. 6. Concentration response of the H_2-LITES sensor. (A) *2f* signal for different H_2 concentrations. (B) The measured *2f* signal amplitude versus H_2 concentration.

noise reduction data is reduced to 10^{-4}, the model stops training and outputs the noise reduction data. In this paper, the measured 2*f* signal of the H_2-LITES sensor at H_2 concentration of 10% is used as an example for the noise reduction process. The results obtained after noise reduction are shown in Fig. 7. The standard deviation (1σ) of the noise is reduced from 1.79×10^{-2} to 4.35×10^{-4} μV when the SNN fitting was employed. On the basis of the signal and noise amplitudes shown in Fig. 7, a minimum detection limit (MDL) of ~80 ppm is obtained for this H_2-LITES sensor.

Heterodyne LITES-based H_2 sensing

The resonance frequency of QTF determines the laser modulation frequency and has a crucial impact on the LITES sensor performance. Therefore, a real-time monitoring of it is needed. In the heterodyne LITES sensor system, a beat frequency signal is generated between the laser modulation frequency, which is detuned from the resonance frequency of QTF, and the transient response of QTF in the resonance state. In such situation, the resonance frequency and the gas concentration can be retrieved simultaneously. Using the modulation strategy shown in Fig. 3B, each period of the varietal sawtooth wave is 2 s and is divided into 2 phases. In the scanning phase, a fast wavelength scanning with 375 ms of time period is adopted to scan across the 4,712.90 cm^{-1} of absorption line. A sine wave is used to modulate the laser wavelength with a non-resonance modulation frequency *f*, where $f = f_0 \pm \Delta f$ and $\Delta f << f_0$. The rise time of the scanning phase is comparable to the response time (~100 ms) of the commercially available QTF, and therefore, a transient response of QTF can be generated. In the stable phase, a pretty long period of 1625 ms is used to acquire the ring-down process of the heterodyne LITES signal. Demodulating the QTF signal at *f* as a function of time, a sinusoidal waveform with exponential decay and period of $\Delta t = 1/\Delta f$ is obtained. Δt can be easily acquired through the measured decay curve. Therefore, $f_0 = f \pm \Delta f$ can be retrieved.

In the subsequent experiments, the integration time of the lock-in amplifier was set to 20 ms, and WMS with the first harmonic (1*f*) detection strategy was adopted. The relationship between the peak signal of the heterodyne LITES sensor and the modulation frequency *f* was investigated and is shown in Fig. 8 together with the resonance curve of the used QTF. The f_0 is measured as 30,713.69 Hz. The signal reached the same amplitude when $f = f_0 \pm \Delta f$. The maximum signal level is obtained when $\Delta f = 3.48$ Hz and $f = 30{,}717.17$ Hz. In the following investigations, these optimum values were employed.

The concentration response of the heterodyne H_2-LITES sensor was investigated and shown in Fig. 9. A constant background baseline of bias was produced because of the residual amplitude modulation when the 1*f* detection method is taken [53]. Furthermore, in the LITES sensor, the laser is modulated. Therefore, the output power changes periodically. This periodically changed power will cause the resonance response of QTF, which produces some offset. With and without (by subtracting) the background, the heterodyne LITES sensor signal versus time was recorded when different H_2 concentrations were used. As shown in Fig. 9A and C, the signal has a decay process. The first positive peak was extracted, and the values versus concentration are plotted in Fig. 9B and D. After linear fitting, the R^2 is recognized as 0.99, which indicates that the heterodyne H_2-LITES sensor has an excellent linear response to H_2 concentration levels.

At an H_2 concentration of 100%, the heterodyne LITES sensor signal was separated from Fig. 9 and is depicted in Fig. 10. The time period Δt between the 2 adjacent positive peaks was found to be 0.2932 s. The resonance frequency can be retrieved in several hundred milliseconds with the measurement accuracy of ±0.2 Hz and the calculated detuning frequency and resonance frequency are $\Delta f = 1/\Delta t = 3.41$ Hz and $f_0 = f - \Delta f = 30{,}713.76$ Hz, respectively. This frequency is almost same as the experimentally obtained result of 30,713.69 Hz shown in Fig. 8. Similar to the denoising operation in the "LITES-based H_2 sensing" section, the SNN is adopted to reduce the system noise level for the heterodyne LITES sensor as well. The noise determination is located at the region where the decay is finished. As presented in the inset of Fig. 10, it can be observed the SNN algorithm effectively suppressed the noise. The noise standard deviation reduced from 54 to 0.13 nV after the algorithm was applied. On the basis of the signal and noise amplitudes shown in Fig. 10, an MDL of ~45 ppm is obtained for this

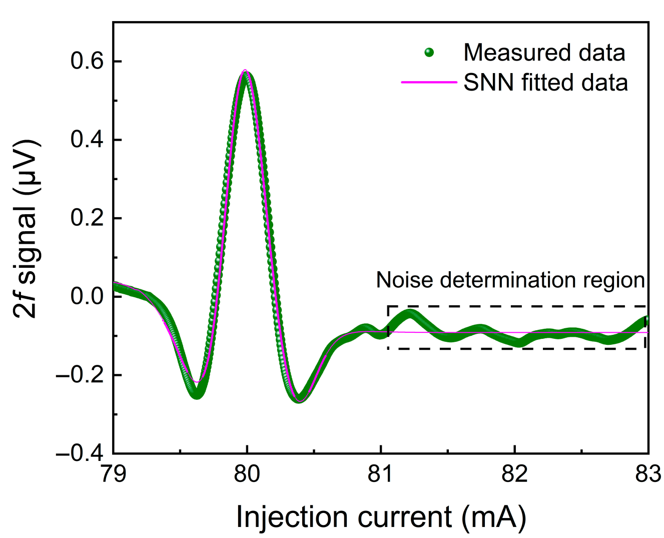

Fig. 7. Denoising for H_2-LITES sensor with the SNN algorithm model at an H_2 concentration of 10%.

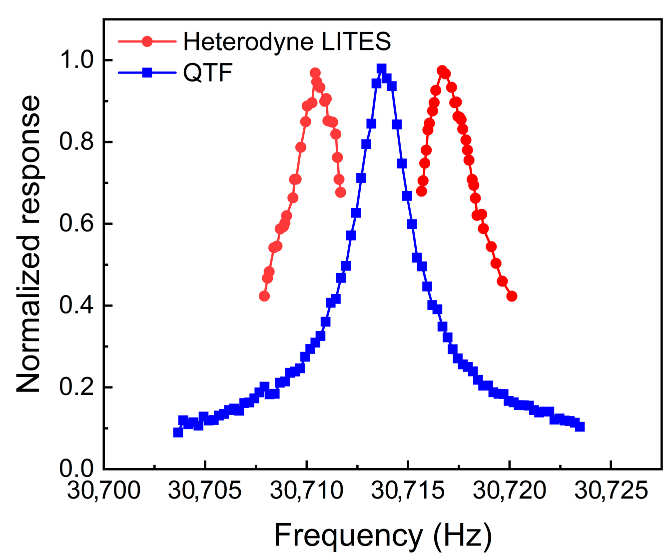

Fig. 8. The normalized signal level of the heterodyne LITES sensor versus the modulation frequency.

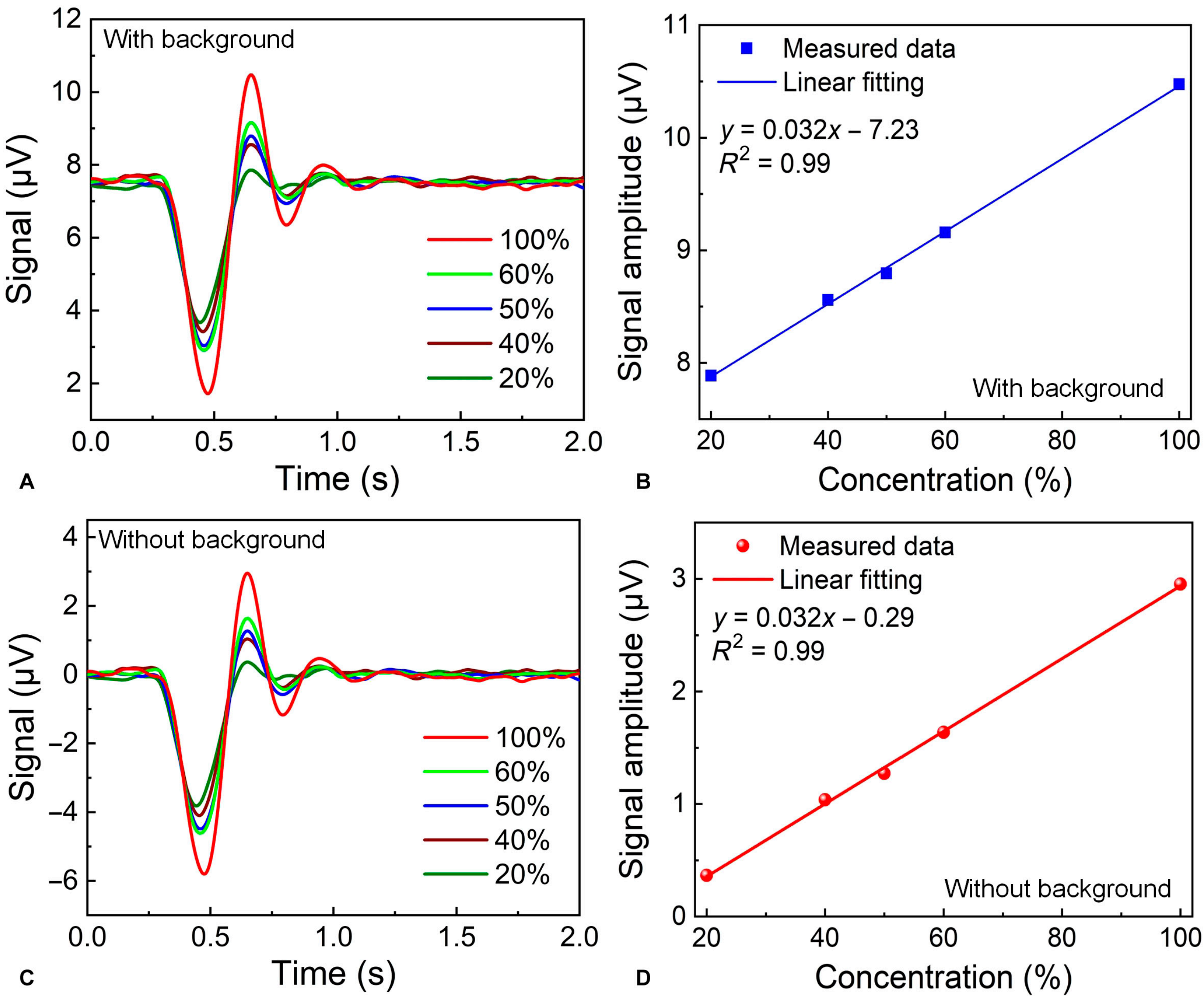

Fig. 9. Concentration response of the heterodyne H_2-LITES sensor. (A) 1*f* signal for different H_2 concentrations with background. (B) The measured signal amplitude versus H_2 concentration with background. (C) 1*f* signal for different H_2 concentrations without background. (D) The measured signal amplitude versus H_2 concentration without background.

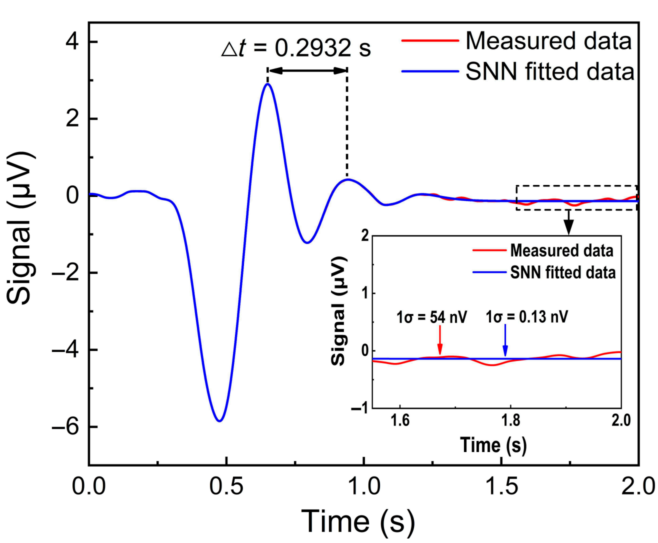

Fig. 10. Denoising for the heterodyne H_2-LITES sensor with the SNN algorithm model.

heterodyne H_2-LITES sensor. For comparison, the reported optical methods for H_2 sensing are listed in Table. Compared with these existing techniques, the LITES and heterodyne LITES-based H_2 sensor have a better performance when MDL is considered.

Conclusion

As a new energy source, H_2 detection has a huge application demand and, therefore, is a research hotspot. In this paper, a highly sensitive H_2 sensor based on LITES technique is presented for the first time. A CW-DFB diode laser with emission in the mid-infrared of 2.1 μm and maximum optical power of 18.4 mW was adopted as the excitation source. The laser has a side–mode suppression ratio of more than 20 dB. The strongest H_2 absorption line located at 4,712.90 cm^{-1} and a Herriott MPC with an optical length of 10.1 m were chosen to meet the challenging problem of weak H_2 absorption. With the feature of processing the raw input data without data preprocessing and extracting the desired features automatically, the robust SNN

Table. The comparison of different optical sensing methods for H_2 detection.

Method	MDL	Ref.
Fiber-tip microcantilever	<1.5%	[15]
Surface plasmon resonance	180 ppm	[14]
TDLAS	0.1%	[23]
TDLAS	0.2%	[24]
LITES	~80 ppm	This work
Heterodyne LITES	~45 ppm	This work

fitting algorithm was brought in to denoise the sensor. For the LITES-based H_2 sensor, it has an excellent linear response to H_2 concentration levels through examining of different gas samples, and the MDL was found to be ~80 ppm. A heterodyne H_2-LITES sensor was further constructed to realize a fast measurement of resonance frequency of QTF and H_2 concentration simultaneously. The retrieved resonance frequency of 30,713.76 Hz is exactly same as the experimentally obtained result of 30,713.69 Hz. After the SNN algorithm was applied, an MDL of ~45 ppm is obtained for this heterodyne H_2-LITES sensor. The sensor performance can be further improved when a laser with a higher output power, an MPC with a longer optical length, or a custom QTF with a lower f_0 is adopted.

Acknowledgments

Funding: This work is supported by the National Natural Science Foundation of China (grant nos. 62275065, 62022032, 61875047, and 61505041) and Fundamental Research Funds for the Central Universities. **Author contributions:** Y.M. conceived the idea, designed the experiments, and supervised the project. T.L. performed the experiment. S.Q. and Z.L. were involved in the discussions. X.L. took part in algorithm analysis. **Competing interests:** The authors declare that they have no conflicts of interest.

Data Availability

The data presented in this study are available on request from the corresponding author.

References

1. Penner SS. Fossil-fuel resources and CO_2 production from combustion. *Energy*. 1991;16(11–12):1417–1419.
2. Midilli A, Ay M, Dincer I, Rosen MA. On hydrogen and hydrogen energy strategies I: Current status and needs. *Renew Sustain Energ Rev*. 2005;9(3):255–271.
3. Mazloomi K, Gomes C. Hydrogen as an energy carrier: Prospects and challenges. *Renew Sust Energ Rev*. 2012;16(5):3024–3033.
4. Pascuzzi S, Blanco I, Anifantis AS, Scarascia-Mugnozza G. Hazards assessment and technical actions due to the production of pressured hydrogen within a pilot photovoltaic-electrolyser-fuel cell power system for agricultural equipment. *J Agric Eng*. 2016;47:88–93.
5. Arora K, Puri NK. Electrophoretically deposited nanostructured PdO thin film for room temperature amperometric H_2 sensing. *Vacuum*. 2018;154:302–308.
6. Hashtroudi H, Yu AM, Juodkazis S, Shafiei M. Ultra-sensitive photo-induced hydrogen gas sensor based on two-dimensional CeO_2-Pd-PDA/rGO heterojunction nanocomposite. *Nanomaterials*. 2022;12(10):1628.
7. Yang F, Kung SC, Cheng M, Hemminger JC, Penner RM. Smaller is faster and more sensitive: The effect of wire size on the detection of hydrogen by single palladium nanowires. *ACS Nano*. 2010;4(9):5233–5244.
8. Yoo SM, Sharma B, Kim JS. Boron nitride nanotubes (BNNTs) decorated Pd-ternary alloy ($Pd_{63.2}Ni_{34.3}CO_{2.5}$) for H_2 sensing. *Int J Hydrog Energy*. 2021;46(22):12263–12270.
9. Chauhan PS, Bhattacharya S. Hydrogen gas sensing methods, materials, and approach to achieve parts per billion level detection: A review. *Int J Hydrog Energy*. 2019;44(47):26076–26099.
10. Zhou LJ, Kato F, Nakamura N, Oshikane Y, Nagakubo A, Ogi H. MEMS hydrogen gas sensor with wireless quartz crystal resonator. *Sens Actuators B Chem*. 2021;334:129651.
11. Boudjiet MT, Bertrand J, Pellet C, Dufour I. New characterization methods for monitoring small resonant frequency variation: Experimental tests in the case of hydrogen detection with uncoated silicon microcantilever-based sensors. *Sens Actuators B Chem*. 2014;199:269–276.
12. Sil D, Hines J, Udeoyo U, Borguet E. Palladium nanoparticle-based surface acoustic wave hydrogen sensor. *ACS Appl Mater Interfaces*. 2015;7(10):5709–5714.
13. Wan JKS, Ioffe MS, Depew MC. A novel acoustic sensing system for on-line hydrogen measurements. *Sens Actuators B Chem*. 1996;32(3):233–237.
14. Cai SS, Gonzalez-Vila A, Zhang XJ, Guo T, Caucheteur C. Palladium-coated plasmonic optical fiber gratings for hydrogen detection. *Opt Lett*. 2019;44(18):4483–4486.
15. Liao CR, Xiong C, Zhao JL, Zou MQ, Zhao YY, Li BZ, Ji P, Cai ZH, Gan ZS, Wang Y, et al. Design and realization of 3D printed fiber-tip microcantilever probes applied to hydrogen sensing. *Light Sci Appl*. 2022;3(1):3–13.
16. Ma YF, Lewicki R, Razeghi M, Tittel FK. QEPAS based ppb-level detection of CO and N_2O using a high power CW DFB-QCL. *Opt Express*. 2013;21(1):1008–1019.
17. Zhang ZH, Zhang FB, Xu B, Xie HQ, Fu BT, Lu X, Zhang N, Yu SP, Yao JP, Cheng Y, et al. High-sensitivity gas detection with air-lasing-assisted coherent Raman spectroscopy. *Ultrafast Sci*. 2022;2022:9761458.
18. Fu Y, Cao JC, Yamanouchi K, Xu HL. Air-laser-based standoff coherent Raman spectrometer. *Ultrafast Sci*. 2022;2022:9867028.
19. Liu XN, Ma YF. Tunable diode laser absorption spectroscopy based temperature measurement with a single diode laser near 1.4 μm. *Sensors*. 2022;22(16):6095.
20. Zhang C, Qiao SD, Ma YF. Highly sensitive photoacoustic acetylene detection based on differential photoacoustic cell with retro-reflection-cavity. *Photo-Dermatology*. 2023;30:100467.
21. Liu YH, Ma YF. Advances in multipass cell for absorption spectroscopy-based trace gas sensing technology. *Chin Opt Lett*. 2023;21(3):033001.
22. Dong L, Tittel FK, Li CG, Sanchez NP, Wu HP, Zheng CT, Yu YJ, Sampaolo A, Griffin RJ. Compact TDLAS based sensor design using interband cascade lasers for mid-IR trace gas sensing. *Opt Express*. 2016;24(6):A528–A535.

23. Avetisov V, Bjoroey O, Wang JY, Geiser P, Paulsen KG. Hydrogen sensor based on tunable diode laser absorption spectroscopy. *Sensors*. 2019;19(23):5313.
24. Liang TT, Qiao SD, Liu XN, Ma YF. Highly sensitive hydrogen sensing based on tunable diode laser absorption spectroscopy with a 2.1 μm diode laser. *Chemosensors*. 2022;10(8):321.
25. Kosterev AA, Bakhirkin YA, Curl RF, Tittel FK. Quartz-enhanced photoacoustic spectroscopy. *Opt Lett*. 2022;27(21):1902–1904.
26. Shang ZJ, Li SZ, Li B, Wu HP, Sampaolo A, Patimisco P, Spagnolo V, Dong L. Quartz-enhanced photoacoustic NH_3 sensor exploiting a large-prong-spacing quartz tuning fork and an optical fiber amplifier for biomedical applications. *Photo-Dermatology*. 2022;26:100363.
27. Lin HY, Zheng HD, Montano BAZ, Wu HP, Giglio M, Sampaolo A, Patimisco P, Zhu WG, Zhong YC, Dong L, et al. Ppb-level gas detection using on-beam quartz-enhanced photoacoustic spectroscopy based on a 28 kHz tuning fork. *Photo-Dermatology*. 2022;25:100321.
28. Sgobba F, Sampaolo A, Patimisco P, Giglio M, Menduni G, Ranieri AC, Hoelzl C, Rossmadl H, Brehm C, Mackowiak V, et al. Compact and portable quartz-enhanced photoacoustic spectroscopy sensor for carbon monoxide environmental monitoring in urban areas. *Photo-Dermatology*. 2022;25:100318.
29. Wang Z, Wang Q, Zhang H, Borri S, Galli I, Sampaolo A, Patimisco P, Spagnolo VL, De Natale P, Ren W. Doubly resonant sub-ppt photoacoustic gas detection with eight decades dynamic range. *Photo-Dermatology*. 2022;27:100387.
30. Patimisco P, Sampaolo A, Zheng HD, Dong L, Tittel FK, Spagnolo V. Quartz–enhanced photoacoustic spectrophones exploiting custom tuning forks: A review. *Adv Phys X*. 2017;2(1):169–187.
31. Menduni G, Zifarelli A, Sampaolo A, Patimisco P, Giglio M, Amoroso N, Wu HP, Dong L, Bellotti R, Spagnolo V. High-concentration methane and ethane QEPAS detection employing partial least squares regression to filter out energy relaxation dependence on gas matrix composition. *Photo-Dermatology*. 2022;26:100349.
32. Dello Russo S, Sampaolo A, Patimisco P, Menduni G, Giglio M, Hoelzl C, Passaro VMN, Wu HP, Dong L, Spagnolo V. Quartz-enhanced photoacoustic spectroscopy exploiting low-frequency tuning forks as a tool to measure the vibrational relaxation rate in gas species. *Photo-Dermatology*. 2021;21:100227.
33. Ma YF, He Y, Zhang LG, Yu X, Zhang JB, Sun R, Tittel FK. Ultra-high sensitive acetylene detection using quartz-enhanced photoacoustic spectroscopy with a fiber amplified diode laser and a 30.72 kHz quartz tuning fork. *Appl Phys Lett*. 2017;110(3):031107.
34. Liu K, Guo XY, Yi HM, Chen WD, Zhang WJ, Gao XM. Off-beam quartz-enhanced photoacoustic spectroscopy. *Opt Lett*. 2009;34(10):1594–1596.
35. Patimisco P, Sampaolo A, Dong L, Tittel FK, Spagnolo V. Recent advances in quartz enhanced photoacoustic sensing. *Appl Phys Rev*. 2018;5(1):011106.
36. Ma YF, He Y, Yu X, Chen C, Sun R, Tittel FK. HCl ppb-level detection based on QEPAS sensor using a low resonance frequency quartz tuning fork. *Sens Actuators B Chem*. 2016;233:388–393.
37. Ma YF, He Y, Tong Y, Yu X, Tittel FK. Quartz-tuning-fork enhanced photothermal spectroscopy for ultra-high sensitive trace gas detection. *Opt Express*. 2018;26(24):32103–32110.
38. Dello Russo S, Zifarelli A, Patimisco P, Sampaolo A, Wei TT, Wu HP, Dong L, Spagnolo V. Light-induced thermo-elastic effect in quartz tuning forks exploited as a photodetector in gas absorption spectroscopy. *Opt Express*. 2020;28(13):19074–19084.
39. Wei TT, Zifarelli A, Dello Russo S, Wu HP, Menduni G, Patimisco P, Sampaolo A, Spagnolo V, Dong L. High and flat spectral responsivity of quartz tuning fork used as infrared photodetector in tunable diode laser spectroscopy. *Appl Phys Rev*. 2021;8(4):041409.
40. Hu LE, Zheng CT, Zhang MH, Zheng KY, Zheng J, Song ZW, Li XY, Zhang Y, Wang YD, Tittel FK. Long-distance in-situ methane detection using near-infrared light-induced thermo-elastic spectroscopy. *Photo-Dermatology*. 2021;21:100230.
41. Liu XN, Qiao SD, Han GW, Liang JX, Ma YF. Highly sensitive HF detection based on absorption enhanced light-induced thermoelastic spectroscopy with a quartz tuning fork of receive and shallow neural network fitting. *Photo-Dermatology*. 2022;28:100422.
42. Hu LE, Zheng CT, Zhang Y, Zheng J, Wang YD, Tittel FK. Compact all-fiber light-induced thermoelastic spectroscopy for gas sensing. *Opt Lett*. 2020;45(7):1894–1897.
43. Qiao SD, Ma PZ, Tsepelin V, Han GW, Liang JX, Ren W, Zheng HD, Ma YF. Super tiny quartz-tuning-fork-based light-induced thermoelastic spectroscopy sensing. *Opt Lett*. 2023;48(2):419–422.
44. Ma YF, He Y, Patimisco P, Sampaolo A, Qiao SD, Yu X, Tittel FK, Spagnolo V. Ultra-high sensitive trace gas detection based on light-induced thermoelastic spectroscopy and a custom quartz tuning fork. *Appl Phys Lett*. 2020;116(1):011103.
45. Qiao SD, Sampaolo A, Patimisco P, Spagnolo V, Ma YF. Ultra-highly sensitive HCl-LITES sensor based on a low-frequency quartz tuning fork and a fiber-coupled multi-pass cell. *Photo-Dermatology*. 2022;27:100381.
46. Ma YF, Hu YQ, Qiao SD, Lang ZT, Liu XN, He Y, Spagnolo V. Quartz tuning forks resonance frequency matching for laser spectroscopy sensing. *Photo-Dermatology*. 2022;25:100329.
47. Wu HP, Dong L, Zheng HD, Yu YJ, Ma WG, Zhang L, Yin WB, Xiao LT, Jia ST, Tittel FK. Beat frequency quartz-enhanced photoacoustic spectroscopy for fast and calibration-free continuous trace-gas monitoring. *Nat Commun*. 2017;8:15331.
48. Gordon IE, Rothman LS, Hargreaves RJ, Hashemi R, Karlovets EV, Skinner FM, Conway EK, Hill C, Kochanov RV, Tan Y, et al. The HITRAN2020 molecular spectroscopic database. *J Quant Spectrosc Radiat Transf*. 2022;277:107949.
49. He Y, Ma YF, Tong Y, Yu X, Tittel FK. Ultra-high sensitive light-induced thermoelastic spectroscopy sensor with a high Q-factor quartz tuning fork and a multipass cell. *Opt Lett*. 2019;44(8):1904–1907.
50. Qiao SD, Ma YF, He Y, Patimisco P, Sampaolo A, Spagnolo V. Ppt level carbon monoxide detection based on light-induced thermoelastic spectroscopy exploring custom quartz tuning forks and a mid-infrared QCL. *Opt Express*. 2021;29(16):25100–25108.
51. Liang N, Sun SS, Zhang C, He Y, Qiu ZJ. Advances in infrared spectroscopy combined with artificial neural network for the authentication and traceability of food. *Crit Rev Food Sci Nutr*. 2022;62(11):2963–2984.
52. Bianchini M, Scarselli F. On the complexity of neural network classifiers: A comparison between shallow and deep architectures. *IEEE Trans Neural Netw Learn Syst*. 2014;25(8):1553–1565.
53. Werle P, Slemr F, Maurer K, Kormann R, Mücke R, Jänker B. Near-and mid-infrared laser-optical sensors for gas analysis. *Opt Lasers Eng*. 2002;37(2–3):101–114.